Limnol. Oceanogr., 54(4), 2009, 1353–1368

Observations of turbulent mixing in a phytoplankton thin layer: Implications for formation, maintenance, and breakdown

Jonah V. Steinbuck,[a,*] Mark T. Stacey,[b] Margaret A. McManus,[c] Olivia M. Cheriton,[d] and John P. Ryan[e]

[a] Environmental Fluid Mechanics Laboratory, Stanford University, Stanford, California
[b] Department of Civil and Environmental Engineering, University of California at Berkeley, Berkeley, California
[c] Department of Oceanography, University of Hawaii at Manoa, Honolulu, Hawaii
[d] Long Marine Laboratory, University of California at Santa Cruz, Santa Cruz, California
[e] Monterey Bay Aquarium Research Institute, Moss Landing, California

Abstract

Coincident measurements of chlorophyll *a* (Chl *a*) and temperature microstructure from Monterey Bay, California, U.S.A., are used to investigate the dynamics of a phytoplankton thin layer in the context of vertical turbulent mixing. The thin layer was situated in the thermocline of a 20.5-m water column, between a strongly turbulent surface mixed layer and a weakly turbulent stratified interior. The differential mixing established an asymmetric layer with a stronger Chl *a* gradient at the base of the layer than at the top. Sinking by *Akashiwo sanguinea* could have balanced turbulent mixing above the layer, but cannot explain the mid-column convergence needed to maintain the thin layer. Swimming by *A. sanguinea* directed towards a mid-column nitracline could have balanced turbulent mixing on both sides of the layer and supported the observed Chl *a* gradients. Results from a Eulerian advection–diffusion model suggest that cell swimming may have varied over the lifetime of the layer, with stronger or more directed swimming required for layer formation and weaker or less directed swimming needed to maintain the layer. In-layer growth is unlikely to have played a primary role in supporting the observed Chl *a* gradients. From the one-dimensional (vertical) observations, the role of shear-induced straining cannot be evaluated, but shear instabilities appear important to forcing elevated rates of turbulent diffusion within the layer. Finally, a Lagrangian particle-tracking model is used to explore the implications of a balance of vertical velocity and turbulent diffusion on the vertical motions of individual cells that constitute the thin layer.

In recent decades, improved spatial resolution of bio-optical and bio-acoustic profiling instrumentation has permitted the study of the fine- to microscale vertical structure of planktonic patchiness in the coastal ocean. Dense layers of plankton with vertical scales of a few meters to decimeters have been observed to span kilometers in the horizontal and persist over hours to days (Dekshenieks et al. 2001; McManus et al. 2003). These thin layers may be characterized by enhanced rates of nutrient uptake, primary production, grazing, and remineralization (Cowles et al. 1998).

A number of physical and biological mechanisms may regulate the dynamics and development of thin layers. Alldredge et al. (2002) found particle buoyancy to be important to the formation of a thin layer of marine snow. Franks (1995) proposed a shear-induced straining mechanism for layer formation, which was further analyzed by Stacey et al. (2007) and Birch et al. (2008). Sullivan et al. (in press) observed thin layers form via vertical migration of the dinoflagellate *Akashiwo sanguinea* (syn. *Gymnodinium sanguineum*). In all cases, the rate of turbulent mixing is likely to play a key role in the layer dynamics (Stacey et al. 2007). Thin layers are typically associated with pycnoclines in which strong density stratification acts to suppress shear instabilities and vertical mixing (Dekshenieks et al. 2001; McManus et al. 2003).

* Corresponding author: vittorio@stanford.edu

In this paper, coincident measurements of chlorophyll *a* (Chl *a*) and temperature microstructure, along with one-dimensional (vertical) numerical models, are used to investigate the physical dynamics of phytoplankton during thin-layer formation, maintenance, and breakdown in Monterey Bay, California, U.S.A. The field component of this work was part of the Layered Organization of the Coastal Ocean (LOCO) project, a multi-institution study aimed at understanding the occurrence and dynamics of planktonic thin layers in the coastal ocean.

Methods

Study site—Monterey Bay is an open embayment, ~37 × 19 km in along-shore and across-shore extent, respectively (Fig. 1). The study site was located in the northern part of the bay (36.9424°N, 121.9409°W), near the 20-m isobath. A number of studies have documented thin layers in this region. During a 2002 study, thin layers comprised of marine viruses, bacteria, phytoplankton, and elongated zooplankton were observed (McManus et al. 2005, 2008; Cheriton et al. 2007). During the LOCO study of 2005, a number of researchers observed thin layers form as a result of the vertical migration of the dinoflagellate *Akashiwo sanguinea* (Sullivan et al. in press; Cheriton et al. 2009).

As observed in other coastal ocean environments, planktonic thin layers in Monterey Bay have been associated with Richardson numbers greater than the critical value of ¼, suggesting that conditions of weak

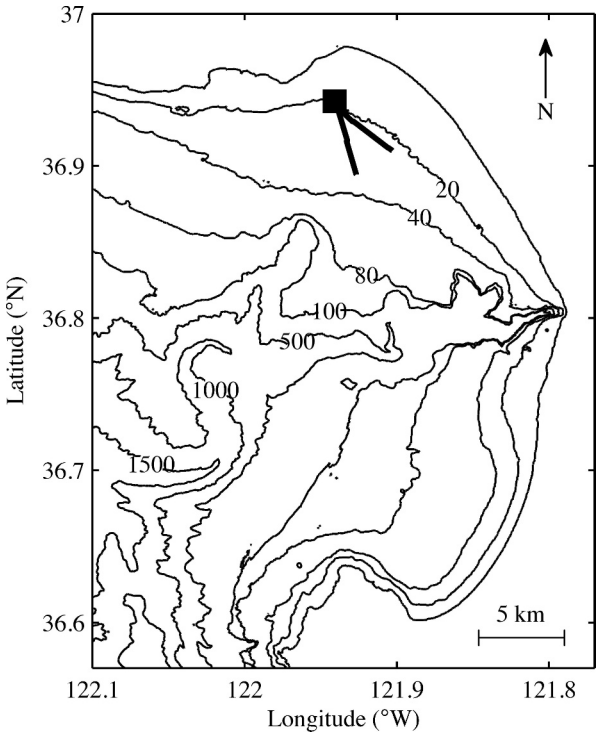

Fig. 1. Map of Monterey Bay, California, U.S.A., with bathymetric contours (m). The study site is marked with a black square at 36.9424°N and 121.9409°W, near the 20-m isobath. The two thick black lines show local segments (within ~5 km of the study site) of the Dorado AUV transect path that was traveled on 18 August and 24 August.

turbulent mixing may be necessary for thin-layer formation and persistence (McManus et al. 2005; Cheriton et al. 2007). On the Monterey Bay continental shelf, the mixing environment is regulated by turbulence production by wind stirring and convection in the surface mixed layer (SML), shear in the bottom boundary layer (BBL), locally generated internal tides, and nonlinear internal waves (Carter et al. 2005). The physical dynamics of the bay are also strongly influenced by the interaction of upwelling with the bay topography. In the northern part of the bay, an upwelling shadow can set up a strongly stratified, cyclonic recirculation zone (Graham and Largier 1997).

Sampling overview—An intensive, multi-institution, multi-investigator field study was conducted from 11 August to 05 September 2005. This paper focuses on observations from a high-resolution profiler and moored acoustic Doppler current profiler (ADCP) during the afternoon of 19 August. A custom-built, free-falling profiler was deployed from a small (10-m) research vessel. The profiler was equipped with a suite of biological and physical instruments, including a WET Labs WETstar fluorometer that measured Chl *a* concentration via fluorescence at 8 Hz, a Biospherical Instruments irradiance sensor that measured photosynthetically active radiation (PAR) at 8 Hz, and a Self-Contained Autonomous Microstructure Profiler (SCAMP, made by Precision Measurement Engineering) that measured temperature, salinity, and pressure at 100 Hz (Carter and Imberger 1986). The profiler was ballasted with floats to maintain a stable vertical orientation and a nominal descent rate of 10 cm s^{-1}. During deployment, a downcast was performed ~ every 4 min, with measurements obtained from 2-m to 17-m depth in a 20.5-m water column. The velocity structure and derived shear were measured using an upward-looking, bottom-mounted 600-kHz Broadband RD Instruments ADCP, located ~50 m from the research vessel. The ADCP measured velocities between ~2-m and 19-m depth with 0.5-m vertical resolution at a sampling rate of 0.2 Hz. The Monterey Bay Aquarium Research Institute Dorado autonomous underwater vehicle (AUV) was also deployed throughout the LOCO study, including 18 August and 24 August, bracketing the period of high-resolution profiling on 19 August. The AUV performed undulating transects (vehicle pitch was 30°) in the northern part of the bay, including segments near the study site (Fig. 1). The AUV was equipped with a suite of sensors including Sea-Bird temperature sensors and an ultraviolet spectrophotometer optical nitrate sensor (Johnson and Needoba 2008), which was calibrated with nitrate measurements from water samples taken during the LOCO study. The details of the data processing and the development of associated numerical models are provided in parallel with the analysis that follows.

Results

Vertical structure of a thin layer and turbulence—On the afternoon of 19 August 2005, a mid-column phytoplankton thin layer was observed within the thermocline (Fig. 2A,B). Salinity variation across the water column was <0.02. The phytoplankton thin layer maintained a similar structure over the 35-min profiling period (10 profiles), which was limited by damage to the free-fall profiler. The thin layer was delineated from the Chl *a* profiles using a gradient threshold technique. The transition points at which the magnitude of the Chl *a* gradient exceeded 6 μg L^{-1} m^{-1} and 14 μg L^{-1} m^{-1} (values tuned for this dataset) were marked as the top and bottom of the layer, respectively (Fig. 2A). The difference in the tolerance was a consequence of an asymmetry in the Chl *a* gradients about the layer centerline. The full-width, half-maximum approach of Dekshenieks et al. (2001) was not appropriate given this asymmetry and the modest variation in magnitude between the Chl *a* peak and background (Fig. 2A). The mean thickness of the layer resulting from this approach was 2.62 m, which included the low-intensity shoulders of the layer (Fig. 2A).

The vertical structure of the layer was examined in the context of its density-stratified, turbulent environment. The competition between stratification and shear was evaluated in terms of the gradient Richardson number,

$$Ri = \frac{N^2}{S^2} \tag{1}$$

where $N^2 = -g/\rho_o(\partial\rho/\partial z)$ is the squared buoyancy frequency (g is the gravitational acceleration and ρ_o and ρ are the mean and spatially variable densities measured by

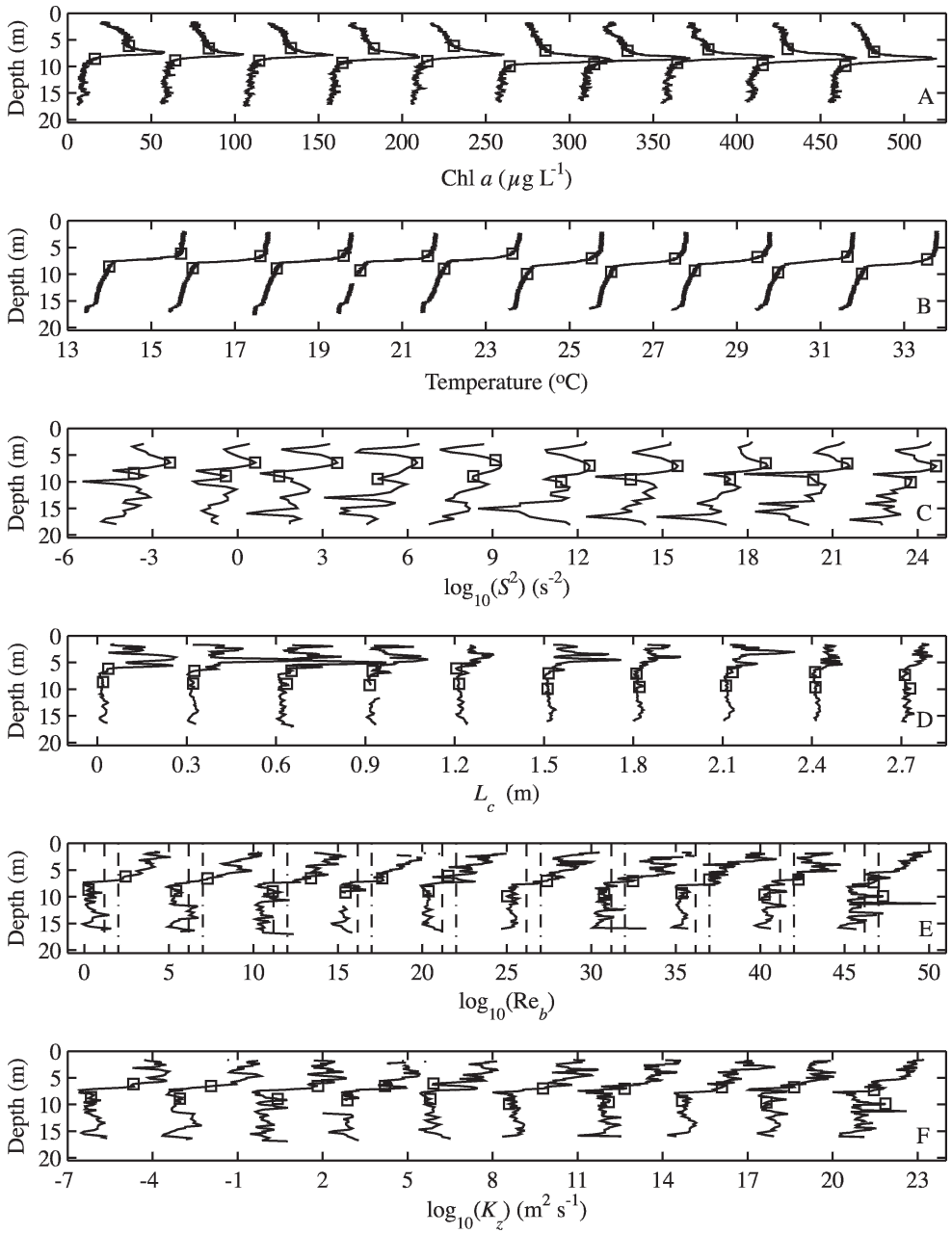

Fig. 2. (A) Profiles of Chl *a* concentration, (B) temperature, (C) squared vertical shear, S^2, (D) centered displacement (overturning) scale, L_c, (E) buoyancy Reynolds number, $\mathrm{Re}_b = \varepsilon/\nu N^2$, and (F) vertical turbulent diffusivity, K_z, for the period 18:12–18:47 h, 19 August 2005. Sequential profiles are offset by (A) 50 μg L^{-1}, (B) 2°C, (C) three orders of magnitude, (D) 0.3 m, (E) five orders of magnitude, and (F) three orders of magnitude. Chl *a* layer edges are marked with square symbols on all panels. Transition values $\mathrm{Re}_b = 15$ (dash) and $\mathrm{Re}_b = 100$ (dash dot) are overlaid in panel (E).

the SCAMP), and where $S^2 = (\partial \bar{U}/\partial z)^2 + (\partial \bar{V}/\partial z)^2$ is the squared vertical shear. The shear was computed by analytically differentiating cubic spline fits to mean horizontal velocity profiles, $\bar{U}$ and $\bar{V}$. A 9-min averaging window was found to capture the primary features of the shear field evident in shorter windows, while providing additional noise reduction. A flow is often considered stable for conditions in which *Ri* exceeds a critical value of ¼ and susceptible to shear instabilities when *Ri* falls below ¼.

The interplay of turbulence and density stratification was evaluated using several metrics. The overturning scale of the turbulence was estimated using the centered displacement scale, L_c, which is given by the root mean square (rms) displacement of water parcels in reordering the density profiles into stable configurations. The salinity

profiles were low-pass filtered to remove salinity spikes prior to estimating density and L_c. The dissipation rate of turbulent kinetic energy, ε, was estimated by fitting a theoretical Batchelor spectrum to the measured temperature gradient spectra from 256 sample (≈25-cm) segments (Batchelor 1959; Gibson and Schwartz 1963). The maximum likelihood fitting approach of Ruddick et al. (2000) was merged with additional noise reduction techniques (Luketina and Imberger, 2001; Steinbuck et al. in press). The competition between turbulence and stratification was then assessed using the buoyancy Reynolds number

$$\mathrm{Re}_b = \frac{\varepsilon}{\nu N^2} \tag{2}$$

where ν is the viscosity. The turbulence is relatively unaffected by stratification for $\mathrm{Re}_b > 100$. Stratification substantially affects the turbulence in the range $15 < \mathrm{Re}_b < 100$ (resulting in anisotropies) and dominates the turbulence for $\mathrm{Re}_b < 15$ (Ivey and Imberger 1991; Itsweire et al. 1993). The dissipation method (Osborn 1980) was used to estimate the vertical turbulent diffusivity

$$K_z = \frac{R_f}{(1-R_f)}\frac{\varepsilon}{N^2} \tag{3}$$

where the flux Richardson number, R_f, was estimated from the measured turbulent Froude number and turbulent Reynolds number (Ivey and Imberger 1991).

The layer was bordered above by an actively turbulent SML with dissipation rates of turbulent kinetic energy, ε, of 10^{-8}–10^{-5} m^2 s^{-3}, and 94% of all values of Re_b above 100, indicating the presence of vigorous, isotropic turbulence (Fig. 2E). The SML was susceptible to shear instabilities (89% of all measured $Ri < ¼$) due to relatively strong shear and weak stratification (Fig. 2B,C). Owing to weak stratification and energetic turbulence, the overturning scales of the turbulence were largest in the SML, on the order of several 10s of cm (Fig. 2D), and turbulent diffusivities were on the order of 10^{-5}–10^{-3} m^2 s^{-1} (Fig. 2F).

The water column underlying the thin layer was relatively quiescent, with ε in the range of 10^{-10}–10^{-9} m^2 s^{-3}, and 85% of all values of Re_b below 15, indicating that stratification dominated the turbulence (Fig. 2E). Due to modest stratification and weak shear (Fig. 2B,C), the flow was mostly stable to shear instabilities (64% of all $Ri > ¼$). The resulting overturning scales were on the order of centimeters (Fig. 2D) and diffusivities were low, primarily on the order of 10^{-6} m^2 s^{-1} (Fig. 2F).

The layer itself was positioned at the interface of the distinct mixing regimes of the SML and quiescent interior. Turbulence intensity parameters within the layer took on characteristics of both regions (Fig. 2). The upper portion of the layer was characterized by turbulence intensities and diffusivities comparable to the overlying SML ($\varepsilon \sim 10^{-8}$–10^{-6} m^2 s^{-3}, $\mathrm{Re}_b > 100$, $K_z \sim 10^{-5}$–10^{-4} m^2 s^{-1}). The lower half of the layer had turbulence conditions similar to the stratified interior ($\varepsilon \sim 10^{-10}$–$10^{-9}$ m^2 s^{-3}, $\mathrm{Re}_b < 15$, $K_z \sim 10^{-6}$ m^2 s^{-1}). Due to the strong stratification within the layer, the overturning length-scales were on the order of centimeters (Fig. 2D). A sharp transition between the two mixing states was collocated with the layer centerline (concentration peak). Due to strong stratification, the flow within the layer was mostly stable to local shear instabilities (68% of all $Ri > ¼$).

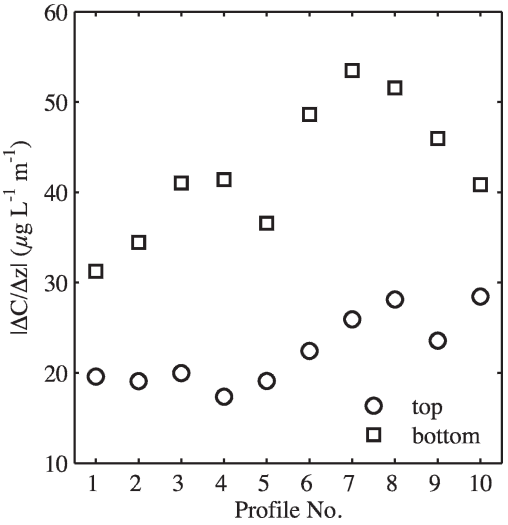

Fig. 3. Magnitude of the vertical gradients of Chl *a* concentration on the top and bottom of the thin layer of Fig. 2A. The gradients were computed from the difference in Chl *a* between the centerline of the layer (concentration maximum) and the top and bottom edges of the layer, respectively.

The vertical structure of the Chl *a* layer exhibited an asymmetry that likely resulted from the vertical variation in turbulent mixing intensity. The Chl *a* gradient of the upper half of the layer was consistently weaker than the gradient on the lower half (Figs. 2A, 3). Strong turbulence at the upper edge of the layer would have acted to mix the phytoplankton-rich layer waters with the less concentrated waters of the SML above, resulting in the relaxation of the Chl *a* gradient. On the lower edge of the layer, on the other hand, weak mixing would have allowed the strong Chl *a* gradient to persist.

Light and nutrients—The thin layer was observed just before sunset on 19 August and, therefore, was found to be present in low light conditions. Near-surface PAR (1-m depth) was 200–300 μmol photons m^{-2} s^{-1} and in-layer PAR was 10–40 μmol photons m^{-2} s^{-1}. Observations made throughout the LOCO study by Sullivan et al. (in press) show that in-layer PAR peaked in daytime layers at $\sim 1.8 \times 10^3$ μmol photons m^{-2} s^{-1} around 14:00 h and decayed to near-zero, nighttime values for layers observed between 20:00 h and 06:00 h.

A mid-column nitracline was observed consistently from Dorado AUV transects throughout the LOCO study (Figs. 1, 4). Nitrate concentrations of <1 μmol L^{-1} were common in the SML and transitioned to values as high as 13 μmol L^{-1} at the base of the 20–30-m-deep water column (Figs. 1, 5), with a mid-column nitracline typically collocated with the thermocline (Figs. 4, 5). Independent measurements made by other researchers in the LOCO study also revealed a mid-column nitracline collocated with

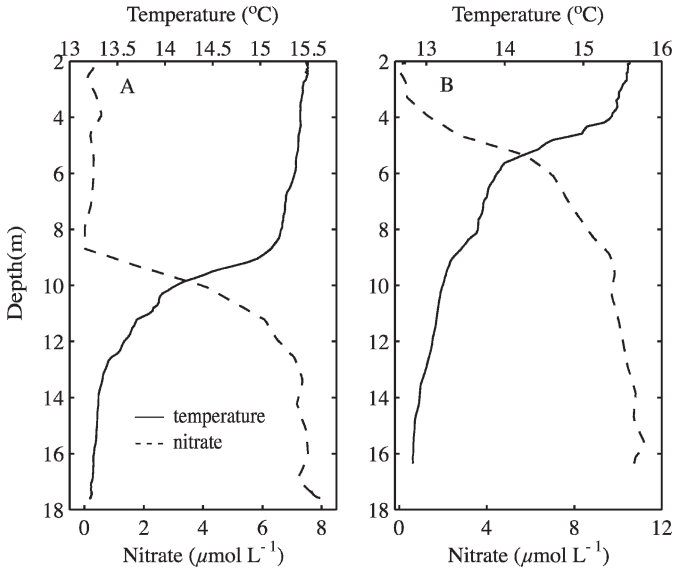

Fig. 4. Sample profiles of nitrate and temperature measured as the Dorado AUV passed the study site (Fig. 1) during two transect surveys bracketing the period of the layer observations on 19 August: (A) 15:04 h on 18 August, and (B) 19:59 h on 24 August.

the thermocline, separating nutrient-depleted surface waters from more replete bottom waters (A. Hanson and P. Egli pers. comm.).

Nitrate had a strong relationship with temperature, which was stationary from 18 August to 24 August, bracketing the period of high-resolution profiling on 19 August (Fig. 5). Johnson and Needoba (2008) observed a similarly strong relationship between nitrate and temperature over a 6-month period in Monterey Bay, with only modest nonstationarity due to biological activity and surface cooling and heating. The condition of stationarity

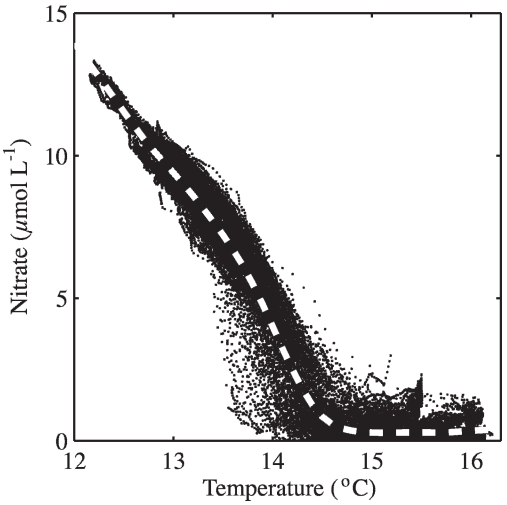

Fig. 5. Nitrate vs. temperature for all Dorado AUV measurements on 18 August (08:43–15:04 h) and 24–25 August (19:59–02:36 h) that were acquired within 5 km of the study site (local depths of ~20–30 m). The white dashed line represents a cubic smoothing spline fit.

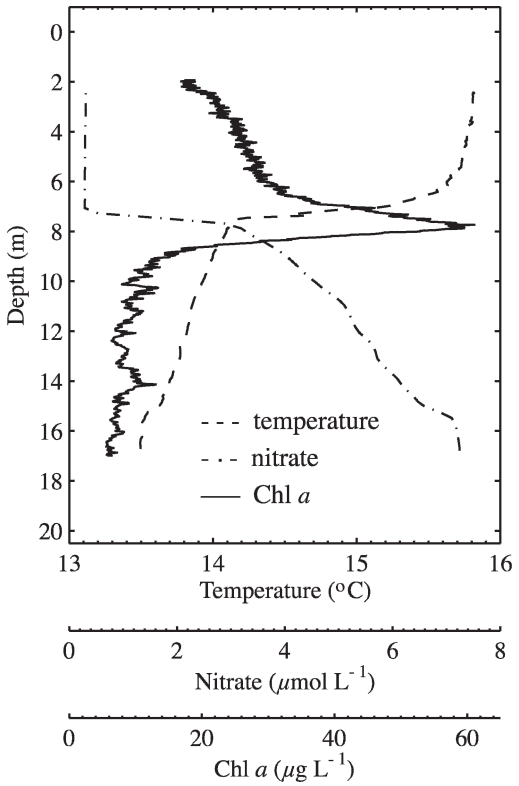

Fig. 6. Sample profiles of observed Chl *a* concentration and observed temperature from 19 August, as well as nitrate inferred from the temperature using the cubic smoothing spline fit from Fig. 5.

allows nitrate to be inferred from direct temperature measurements acquired during the layer observations on 19 August, using a cubic smoothing spline fit to the data (Fig. 5). The inferred nitrate profiles suggest that the Chl *a* layer on 19 August was collocated with a mid-column nitracline (Fig. 6). The nitracline could have provided a migration target for the motile organisms or a region conducive to phytoplankton growth. These mechanisms for phytoplankton thin-layer formation, in addition to cell buoyancy and shear-induced straining, are considered in the following sections. The viability and implications of various dynamic balances is evaluated in terms of the timescales of layer development and the vertical motions of individual cells.

Swimming and buoyancy—During the LOCO study of 2005, Sullivan et al. (in press) observed thin layers form via diurnal vertical migration by *Akashiwo sanguinea*. They found that these dinoflagellates typically aggregated near the surface during the day and in the pycnocline and nutricline at night, though the migrations were asynchronous with sunrise and sunset. In addition to phototaxis and geotaxis, they suggested that circadian rhythms and metabolic requirements may have also played a role in the migration behavior (Kamykowski and Yamazaki 1997; Kamykowski et al. 1998). Further, asymmetries in migration ascent and descent rates were observed, possibly due to the negative buoyancy of the cells.

Both swimming and cell buoyancy may provide convergences of plankton available to counteract the diffusive effects of turbulence and maintain a thin layer (Stacey et al. 2007). To examine the potential role of swimming and cell buoyancy in the dynamics of the layer in the present study, we consider a steady balance of vertical velocity and turbulent diffusion

$$\frac{\partial}{\partial z}(wC) = \frac{\partial}{\partial z}(K_z \frac{\partial C}{\partial z}) \quad (4)$$

where C is the concentration of biological material and w is its vertical velocity. The solution for the concentration profile may be written in the form

$$\ln(\frac{C}{C_o}) = \int \frac{w}{K_z} dz \quad (5)$$

where C_o is the maximum concentration. An estimate of the vertical velocity required to maintain a steady layer structure in the presence of turbulent mixing was computed by differentiating Eq. 5

$$w = K_z \frac{\partial}{\partial z}\left[\ln(\frac{C}{C_o})\right] \quad (6)$$

Analytical differentiation was carried out on polynomial fits to $\ln(C/C_o)$, with C taken as the concentration of Chl *a*. We note that the variation in the Chl *a* gradients within the profiles required that we perform piece-wise polynomial fits of variable order. The measured diffusivity profiles (Fig. 2F) were used for K_z in Eq. 6.

The resulting inferred vertical velocities in the upper water column are oriented downwards and are relatively large in magnitude, with median values primarily in the range 10^{-3}–10^{-2} mm s^{-1} (Fig. 7). In contrast, the inferred vertical velocities in the lower water column are oriented upwards, with a magnitude of 10^{-3} mm s^{-1} at the base of the layer and 10^{-5}–10^{-4} mm s^{-1} lower in the water column (Fig. 7). The inferred velocity profile decays in magnitude within the layer and switches sign about the center of the layer (Fig. 7). The convergent fluxes of Chl *a* into the layer due to the inferred vertical velocity balances the divergent fluxes associated with turbulent diffusion, as expressed in Eq. 4.

In Fig. 7, the inferred vertical velocities are compared to estimates of the swimming and sinking speeds for *Akashiwo sanguinea*. Although the phytoplankton community was diverse during the LOCO study of 2005, the motile dinoflagellate *A. sanguinea* is thought to have been the dominant species responsible for the formation of thin layers (Sullivan et al. in press). The maximum swim speed, w_{swim}, was taken as 3×10^{-1} mm s^{-1}, based on the laboratory measurements of Park et al. (2002). The sinking speed of *A. sanguinea*, w_{sink}, was taken as 2.3×10^{-2} mm s^{-1}, which represents a mean derived from various laboratory estimation techniques (Kamykowski et al. 1992). Another estimate of the sinking speed was calculated using Stokes' law (Kundu and Cohen 2004)

$$w_{Stokes} = \frac{\Delta\rho g D^2}{18\rho_o v} \quad (7)$$

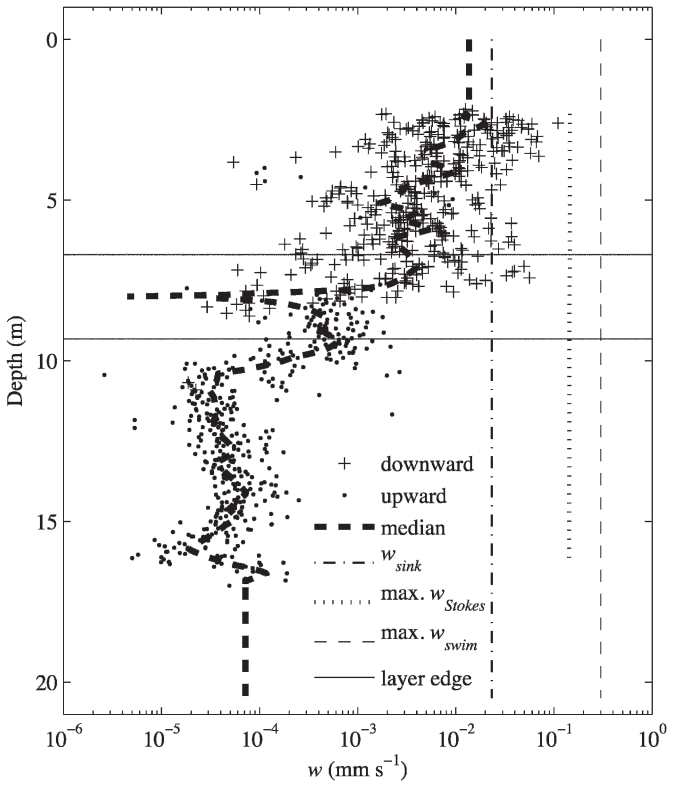

Fig. 7. Vertical velocity, w, inferred from a vertical velocity–diffusion balance (Eqs. 4, 6), using the Chl *a* and K_z profiles of Fig. 2. The median profile is extended with nearest-value extrapolation to the water column boundaries. Laboratory estimates of sinking speed for *Akashiwo sanguinea* (w_{sink}; Kamykowski et al. 1992), maximum Stokes settling speed (max. w_{Stokes}), and maximum expected swim speed (max. w_{swim}; Park et al. 2002) are overlaid for comparison. The max. w_{Stokes} was determined from Eq. 7, using a cell diameter of 75 μm and a cell density of 1073 kg m^{-3} (Kamykowski et al. 1992). Mean position of the top and bottom Chl *a* layer edges are overlaid.

where $\Delta\rho$ is the difference in density between the *A. sanguinea* cells (1073 kg m^{-3}; Kamykowski et al. 1992) and the surrounding seawater, ρ_o is an ambient density, and D is the cell diameter. The shape of *A. sanguinea* is somewhat elliptical and the size is variable within a given population and depends on cell division and the phase of growth, among other factors. An upper bound on w_{Stokes} was estimated using an equivalent spherical diameter of 75 μm, which was the largest dimension of individual *A. sanguinea* cells taken from water samples during the LOCO study (J. Rines pers. comm.). Cloern and Dufford (2005) found *A. sanguinea* to have a mean equivalent spherical diameter of 61 μm in San Francisco Bay, further suggesting that 75 μm is likely an overestimate. The resulting upper bound for w_{Stokes} is $\sim 1.4 \times 10^{-1}$ mm s^{-1}.

Both the laboratory estimate of the sinking speed for *Akashiwo sanguinea*, w_{sink}, and the upper bound Stokes sinking velocity, w_{Stokes}, are sufficiently large to explain the downward vertical velocity in the upper water column (Fig. 7). However, the inferred upward velocity in the lower water column and the resulting mid-column convergence

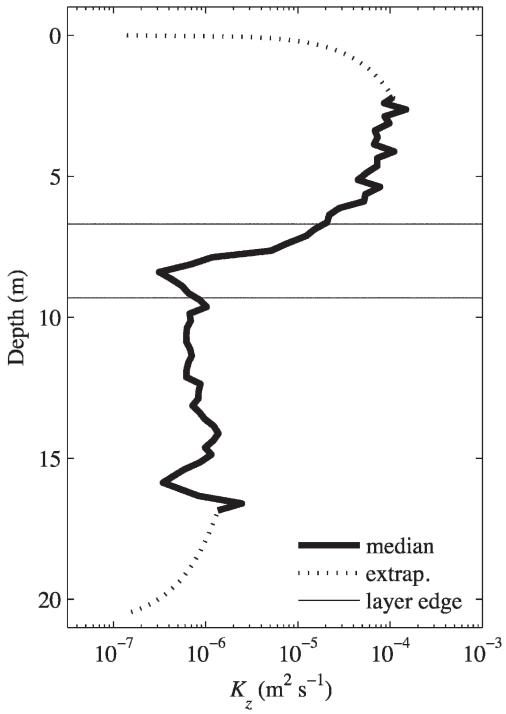

Fig. 8. Median vertical turbulent diffusivity, K_z, from the 10 measured profiles in Fig. 2F with linear extrapolation to 1.4×10^{-7} m^2 s^{-1} at the water column boundaries. Mean position of the top and bottom edges of the Chl *a* layer are overlaid.

within the layer cannot be explained by the sinking of *A. sanguinea*. The variation in w_{Stokes} due to density variations across the thermocline is only about 1% (this is essentially imperceptible in Fig. 7). Thus, sinking alone could not have produced the convergence that is needed to support the observed layer structure.

The maximum swim speed of *A. sanguinea*, w_{swim}, is sufficiently large to explain the inferred velocities throughout the water column, both above and below the layer centerline. Thus, swimming by these dinoflagellates alone could have maintained the layer structure. Note, the results are consistent with the expectation that the magnitude of the vertical velocity for Chl *a* concentration (representing the aggregation of many cells with variable orientation) be smaller than the swim speed potential of an individual cell. Differences between swim speed potential and the effective vertical swim speed may be attributed to random components in the swimming of flagellates as well as reorientation of cells by small-scale shear (Kessler 1986; Bearon et al. 2004; Kiørboe et al. 2004).

Considering a combination of sinking and swimming by *A. sanguinea*, it may be observed that the sinking velocity, w_{sink}, in the upper water column is comparable to the inferred velocity, so only relatively weak swimming (if any) is needed to maintain the layer. In the lower water column, on the other hand, relatively strong upward swimming would be required to offset the sinking velocity and maintain the inferred upward velocity (Fig. 7).

A one-dimensional (vertical) Eulerian advection–diffusion model was developed to investigate the temporal development of the layer forced by vertical velocity and diffusion. The model included unsteadiness, and time-invariant, vertically variable vertical velocity and turbulent diffusion

$$\frac{\partial C}{\partial t} + \frac{\partial}{\partial z}(wC) = \frac{\partial}{\partial z}\left(K_z \frac{\partial C}{\partial z}\right) \tag{8}$$

The solution for the Chl *a* concentration profile, $C(z)$, was advanced in time with the explicit (forward) Euler method and the vertical gradients were computed using a simple forward difference scheme. The no-flux boundary conditions were enforced at the sea surface and bed. A time step of 1 s was found to be suitable for obtaining stable, accurate solutions.

The formation of the layer was considered first by taking the median-inferred vertical velocities as a description of the Chl *a* velocity and using the median diffusivity profile with extrapolation (Figs. 7, 8). The modeled evolution of a hyperbolic tangent Chl *a* profile produces a good match with the observed layer structure, supporting the inferred velocity profile (Figs. 7, 9). However, the model results show that ~6 d are required for the observed layer structure to develop (Fig. 9). Observations made by other researchers in the LOCO study suggest that the timescale of mid-column layer formation by *A. sanguinea* migration was a few hours (Sullivan et al. in press). Thus, the inferred vertical velocities appear insufficient to form the layer in the observed timescale. By forcing the model instead with an elevated swim speed above the layer centerline, the timescale of formation is rapidly reduced. For example, the modeled peak in-layer concentration can match the observed peak within ~8 h with a vertical velocity, w, which is 5% of w_{swim} (1.5×10^{-2} mm s^{-1}), 2.5 h for 10% of w_{swim} (3×10^{-2} mm s^{-1}), and 0.6 h for 20% of w_{swim} (6×10^{-2} mm s^{-1}; Fig. 10). Thus, stronger swimming, or more vertically directed swimming, in the upper water column may have been occurring during the layer formation phase. The fractions of the swim potential w_{swim} considered here are intended to account for variations in the effective vertical speed of the cells due to variably directed swimming, tumbling, and reorientation by small-scale shear (Bearon and Pedley 2000; Bearon et al. 2004; Bearon and Grümbaum 2008). Also, note that the elevated cell velocities in the upper water column produce Chl *a* layers that are thinner than in the field observations (Fig. 10), suggesting that the velocity must subsequently relax in order for the broader observed layer structure to develop.

Cell buoyancy may have also played a role in the layer formation. For $w = w_{sink}$ (~2×10^{-2} mm s^{-1}) prescribed only above the layer, the modeled in-layer peak can match the observations in ~5 h, which is of the same order as the mid-column layer development observed by Sullivan et al. (in press). However, as mentioned previously, sinking in the absence of swimming should actually produce a nearly uniform vertical velocity profile throughout the entire water column, with only ~1% variation due to ~1% variation in density across the thermocline. Eulerian model runs with the vertical velocity set to w_{Stokes} reveal that the convergence associated with this ~1% variation in sinking speed within the thermocline is far too small to produce or

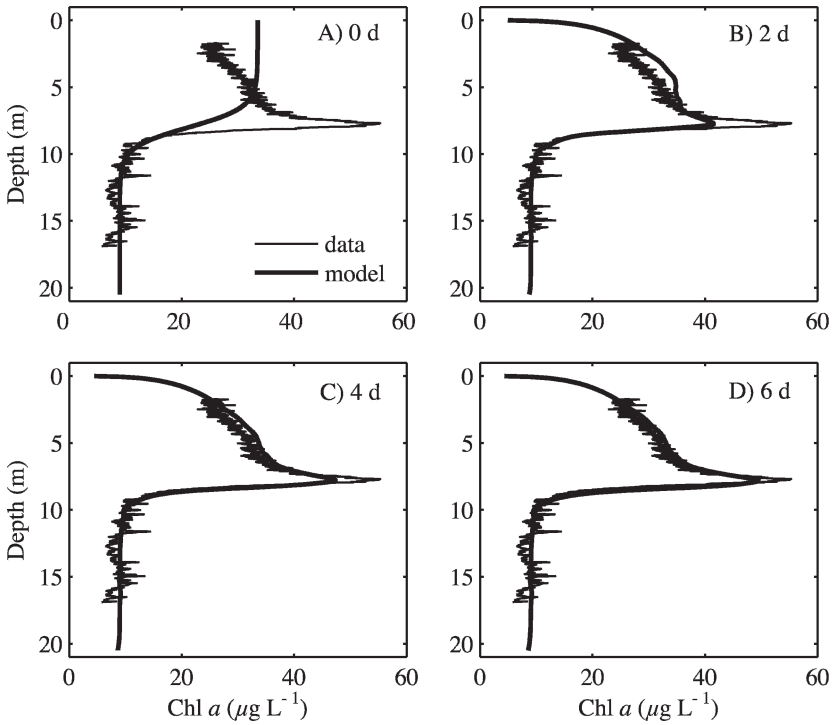

Fig. 9. Sample profiles of observed and modeled Chl *a* concentration showing the formation of a thin layer under the action of vertical cell velocity and diffusion. The Eulerian advection–diffusion model was initialized with a hyperbolic tangent Chl *a* profile and forced with the inferred vertical velocity profile and median observed diffusivity profile with extrapolation to the water column boundaries (Figs. 7, 8). The model results are shown at (A) 0 d, (B) 2 d, (C) 4 d, and (D) 6 d, along with a sample observed profile (same for all panels). The timescale of layer formation is ~6 d.

maintain a thin layer in the presence of turbulent diffusion. For example, a hypothetical hyperbolic tangent profile (as in Figs. 9 and 10) evolves into a broad, downward-moving, concentration maximum. Similarly, for an initially thin surface patch, sinking and turbulence produce a broad, downward-moving patch, not a thin layer. Thus, particle buoyancy alone cannot produce the mid-column convergence required to maintain the thin layer and another mechanism such as convergent swimming is required.

The vertical velocity inferences of this study in combination with the observations of other LOCO research groups in Monterey Bay in 2005 (Sullivan et al. in press) suggest that swimming, perhaps in combination with sinking, is a valid mechanism for layer formation and maintenance. Still, other mechanisms may have been important to the layer dynamics of 19 August. In the following sections, the potential role of phytoplankton growth and shear-induced straining is considered.

In-layer growth

Given that the thin layer was positioned in the middle of the water column, where both nutrients and light may be sufficient for in-layer growth, the combination of growth and diffusion was evaluated as a candidate balance to explain the observed thin layer. Growth and mortality may provide a local source or sink of Chl *a* that balances the vertical turbulent fluxes:

$$0 = \frac{\partial}{\partial z}\left(K_z \frac{\partial C}{\partial z}\right) + \mu_{net} C \tag{9}$$

Estimates of the net rate of production of Chl *a*, μ_{net}, were determined from the observed Chl *a* and diffusivity profiles using (Eq. 9). Due to the sensitivity of the calculation to microscale ($<$ a few centimeters) vertical variability, the profiles were first smoothed. The median diffusivity profile of Fig. 8 was used for K_z. The Chl *a* profiles, $C(z)$, were smoothed using the Eulerian model and a tuned estimate of the profile of μ_{net} that maintained the finescale ($>O$[10 cm]) structure of the Chl *a* profile, while smoothing the microscale variability. An estimate of μ_{net} was then estimated by directly computing the diffusive fluxes of Eq. 9 using a difference estimate for the derivatives (Fig. 11).

The inferred production rates of Chl *a*, μ_{net}, show elevated rates of production ($\mu_{\text{net}} > 0$) near the layer centerline needed to maintain a layer peak, while elevated loss rates ($\mu_{\text{net}} < 0$) are needed on the layer top and bottom to maintain the Chl *a* gradients at the layer edges (Fig. 11). The net production rates are several orders of magnitude higher around the layer and in the upper water column compared to the lower water column owing to the difference in the magnitude of the turbulent fluxes.

Although μ_{net} represents the net production rate of Chl *a*, we note that for a fixed Chl : carbon ratio, the inferred μ_{net}

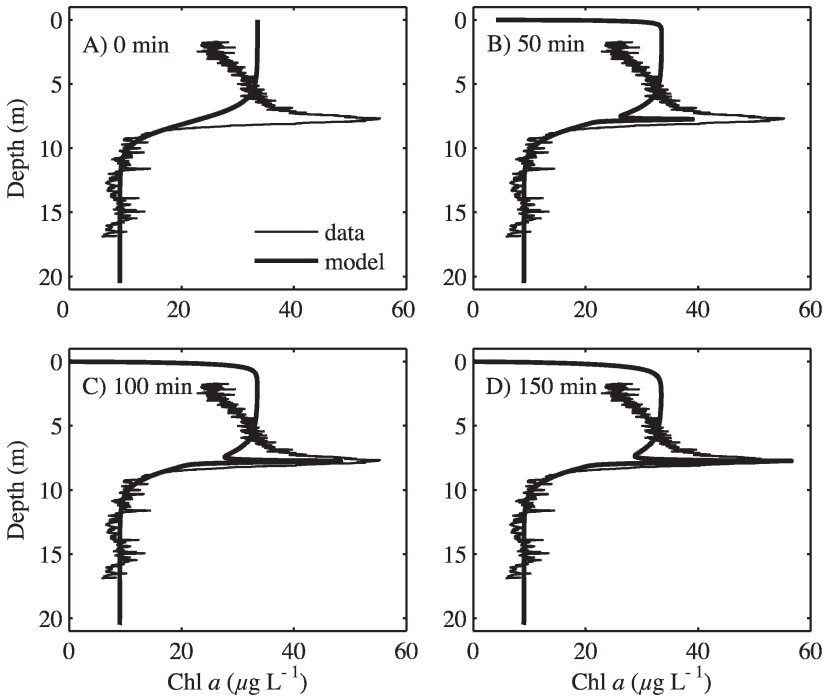

Fig. 10. Sample profiles of observed and modeled Chl *a* concentration showing the formation of a thin layer for rapid downward swimming. The Eulerian advection–diffusion model was initialized with a hyperbolic tangent Chl *a* profile and forced with the observed diffusivity with extrapolation (Fig. 8), the inferred vertical velocity below the layer centerline (Fig. 7), and a constant downward velocity of 3×10^{-2} mm s^{-1} (10% of w_{swim}; Park et al. 2002) above the layer centerline. The model results are shown at (A) 0 min, (B) 50 min, (C) 100 min, and (D) 150 min, along with a sample observed profile (same for all panels). The timescale of layer formation is ~2.5 h.

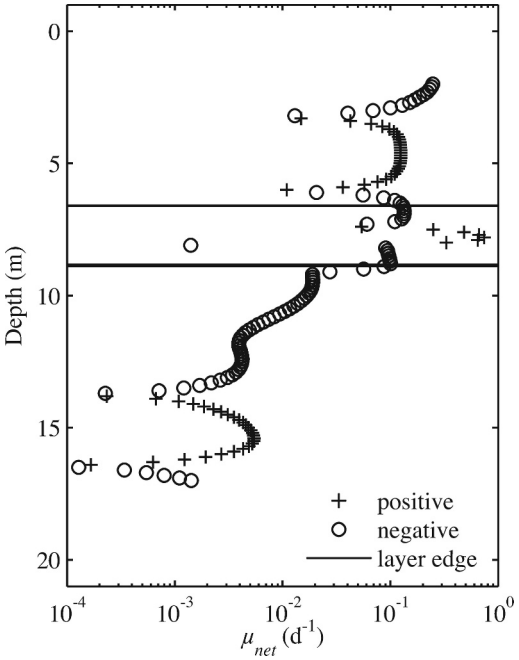

Fig. 11. Sample profile of inferred net production rate of Chl *a*, μ_{net}, calculated for a growth–diffusion balance described by Eq. 9. Positive values of μ_{net} indicate that the rate of production of Chl *a* exceeds the rate of loss, while negative values indicate the opposite. Chl *a* layer edges have been overlaid.

would also correspond to the net growth rate of phytoplankton carbon. Assuming a fixed Chl : carbon ratio (Cloern et al. 1995), it is interesting to note that the inferred growth rate at the center of the layer, $\mu_{net} \approx 7 \times 10^{-1}$ d^{-1}, exceeds the maximum measured growth rate for *Akashiwo sanguinea*, 3.4–3.8 $\times 10^{-1}$ d^{-1} (Doucette and Harrison 1990). This suggests that growth of *A. Sanguinea* alone is unlikely to be able to maintain (or form) the observed structure.

To evaluate the unsteady development of the thin layer subject to growth and diffusion, the Eulerian model was forced as follows (Sharples 2008):

$$\frac{\partial C}{\partial t} = \frac{\partial}{\partial z}(K_z \frac{\partial C}{\partial z}) + \mu_{net} C \tag{10}$$

where the concentration of Chl *a*, $C(z)$, is assumed to be present in neutrally buoyant cells and where the μ_{net} and K_z are taken from Figs. 8, 11. A hypothetical hyperbolic tangent profile for Chl *a* evolves into the observed profile, supporting the inferred net production rates, μ_{net} (Figs. 11, 12). The timescale of layer formation is ~6 d (Fig. 12). Interestingly, the timescale of layer formation due to inferred growth (Fig. 12) is similar to that for inferred vertical velocity (Fig. 9), which is likely due to the fact both mechanisms must produce comparable terms in the advection–diffusion equation in order to balance the same diffusive fluxes (Eqs. 4, 9). Given that the timescale to layer formation due to in-layer growth is on the order of days

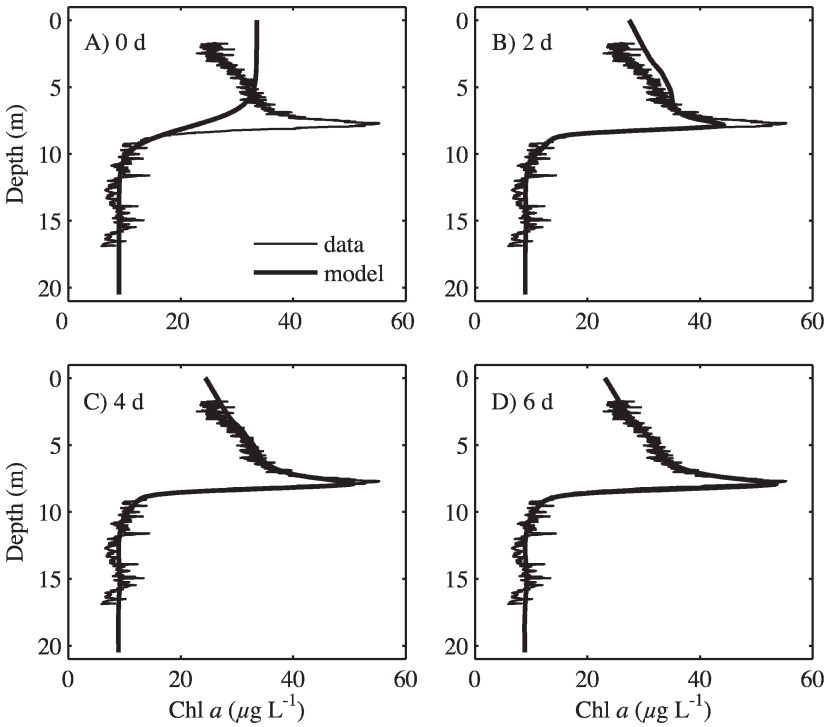

Fig. 12. Sample profiles of observed and modeled Chl *a* concentration showing the formation of a thin layer via growth and diffusion. The Eulerian advection–diffusion model was initialized with a hyperbolic tangent Chl *a* profile and forced with the observed diffusivity with extrapolation (Fig. 8) and the inferred net production rate for Chl *a*, μ_{net} (Fig. 11). The model results are shown at (A) 0 d, (B) 2 d, (C) 4 d, and (D) 6 d, along with a sample observed profile (same for all panels). The timescale of layer formation is ~6 d.

and that higher rates of in-layer growth are likely unrealistic, cell growth and mortality may have played a secondary role in the layer dynamics occurring over timescales of 10s of hours and less.

Shear and straining—Another mechanism for the formation of layers is shear-induced straining. The vertical shear in the horizontal velocities was enhanced at the top edge of the layer (Fig. 2C), indicating that straining may have played a role in the layer dynamics. Ryan et al. (2008) observed thin phytoplankton layers in Monterey Bay within sharp transitions in flow direction, with the strength of the vertical shear negatively correlated with layer thickness and the peak shear occurring at the layer center. Shear may produce thin layers directly by straining a horizontal patch of plankton (Franks 1995; Stacey et al. 2007; Birch et al. 2008). Alternatively, shear may act to indirectly support layer formation, for example by straining the density field and maintaining the relatively high mid-column stratification. In either case, the straining process depends on the advection of horizontal gradients. For example, the unsteady development of a thin layer subject to straining and vertical diffusion may be modeled as

$$\frac{\partial C}{\partial t} + \frac{\partial}{\partial x}(uC) = \frac{\partial}{\partial z}\left(K_z \frac{\partial C}{\partial z}\right) \tag{11}$$

Given the limitations of the layer observations, including the lack of information on the horizontal structure and evolution of the phytoplankton concentration field, it is not possible to evaluate whether the shear produced relevant straining. However, the one-dimensional (vertical) observations do suggest that shear instabilities forced the turbulent mixing (*see* section on the vertical structure of a thin layer and turbulence above), and therefore indirectly supported a diffusive divergence, as discussed for example in Stacey et al. (2007).

Dynamics of individual cells during layer maintenance—To further evaluate the potential dynamics of individual cells during layer maintenance, a one-dimensional (vertical) Lagrangian particle-tracking model was developed. Here, the discussion is focused on the implications of a potential swimming-buoyancy–diffusion balance. The Lagrangian model followed closely from Visser (1997), Batchelder et al. (2002), and Ross and Sharples (2004). Within a given time step, cell positions were updated over several substeps. First, the cells were advected according to their individual vertical velocity due to swimming and/or buoyancy, w_{sb}. Second, the cells underwent nonrandom 'advection' from regions of low to high diffusivity to prevent spurious aggregation (Visser 1997). Both of these steps were accomplished using fourth-order Runge–Kutta advancement (Batchelder et al. 2002). The cells were then

diffused with a random walk step with a magnitude that was based on the diffusivity, K_z, present at the mean cell position from the first two sub-steps. The completion of the time step included a reflection boundary condition at the sea surface and seafloor (Ross and Sharples 2004). The updating of each cell's position may then be expressed as follows:

$$z^{(0)} = z_{n-1} + w_{sb}\Delta t \tag{12}$$

$$z^{(1)} = z^{(0)} + K_{z'}\left(z^{(0)}\right)\Delta t \tag{13}$$

$$z^{(2)} = z^{(1)} + \zeta_n \sqrt{2K_z(\frac{1}{2}[z^{(1)} + z^{(0)}])\Delta t} \tag{14}$$

$$z_n = \begin{cases} -z^{(2)} & z^{(2)} < 0 \\ z^{(2)} & 0 < z^{(2)} < H \\ 2H - z^{(2)} & z^{(2)} > H \end{cases} \tag{15}$$

where z_{n-1} is the initial particle position, $z^{(i)}$ (i = 0, 1, 2) are intermediate positions, z_n is the final position, K_z' is the vertical gradient of the diffusivity, ζ_n is a random variable with unit variance, Δt is the time step, and H is the total water column depth. The observed median diffusivity profile from the 10 measured profiles (Fig. 8) was used to force Eqs. 13, 14. The median operation provided smoothing that improved the behavior of the diffusivity gradient (Ross and Sharples 2004). A time step of 10 s was found to be sufficiently small to give accurate results.

A simple model of the vertical cell velocity due to swimming and buoyancy, w_{sb}, was employed. More complex models of swim behavior have been developed based on the modeled internal state of the cells, for example the cellular carbon : nitrogen ratio (Ross and Sharples 2007, 2008). This approach was not pursued, because many unknown parameters must be assumed and the timescale of layer maintenance is expected to be small compared to the timescales of nitrogen uptake and drawdown within a cell. Instead, cells were simply marked as either actively moving due to swimming and/or buoyancy (referred to as 'motile') or not (referred to as 'passive'). By this definition, w_{sb} = 0 for passive cells. For motile cells, w_{sb} is set such that the mean cell velocity (including both motile and passive cells) at a given depth matches the inferred vertical velocity profile (Fig. 7). Thus, as the fraction of motile cells decreases, the motile cells are required to move faster. The combined swimming-buoyancy vertical velocity of the cells may then be expressed as

$$w_{sb}(z) = \begin{cases} \dfrac{1}{f_{motile}(z)}\alpha w(z) & \text{motile} \\ 0 & \text{passive} \end{cases} \tag{16}$$

where $f_{motile}(z)$ is the local fraction of motile cells, $w(z)$ is the local inferred vertical velocity (Fig. 7), and α is a parameter that allows minor tuning to the median estimate for $w(z)$ so as to optimize the match between a given observed Chl *a* profile and the modeled Chl *a* profile at steady state. In the example discussed below, α = 1.5, which represents very slight tuning, given the order of magnitude variations in $w(z)$ through the water column. It is also important to note that the migration oriented towards the layer centerline described by $w(z)$ (Fig. 7) is likely consistent with migration towards the base of a nitracline (Figs. 4, 5, 6). For all profiles of Chl *a* and inferred nitrate for 19 August, the Chl *a* peak was within ±0.3 m of the base of the inferred nitracline (e.g., Fig. 6).

The model was initialized with observed Chl *a* profiles seeded with 10,000 cells, assuming a linear relationship between Chl *a* concentration and cell abundance. Here, three model scenarios with different fractions of motile cells are considered: f_{motile} = 1.0 (100% motile), f_{motile} = 0.75 (75% motile), and f_{motile} = 0.5 (50% motile). As mentioned previously, the individual motile cell velocities must increase as the fraction of motile cells f_{motile} decreases (Eq. 16). For the three scenarios considered, the maximum swimming-buoyancy cell velocities, w_{sb}, occur in the upper water column and are $\sim 3 \times 10^{-2}$ mm s^{-1} for f_{motile} = 1.0, 3×10^{-1} mm s^{-1} for f_{motile} = 0.75, and 6×10^{-1} mm s^{-1} for f_{motile} = 0.5. Recall, the potential swimming and sinking speeds for *Akashiwo sanguinea* are $\sim 3 \times 10^{-1}$ mm s^{-1} and 2×10^{-2} mm s^{-1}, respectively (Kamykowski et al. 1992; Park et al. 2002). Thus, model runs with an f_{motile} value of around 0.5 and below produce some occurrences of unrealistic vertical cell velocities in the upper water column.

The model runs were allowed to spin up for 48 h to avoid transient behavior associated with the initialization of the specific cells that were marked as motile and passive, which was randomized. The statistics of the cell trajectories were then computed based on a 120-h model period. This 120-h model period exceeds the expected mid-column layer lifetime (<10 h) based on the observations of Sullivan et al. (in press), but allows for the calculation of more robust statistics of the cell trajectories. For each model scenario, the prescription of Eq. 16 produced a steady-state modeled Chl *a* profile that matched the observed Chl *a* profile (Fig. 13). This indicates that a range of swim behaviors can maintain the observed layer structure in a steady state as long as the mean cell velocities match the inferred vertical velocity profile (Fig. 7).

The Lagrangian model results indicate that in the upper water column, cells typically fluctuated between the layer and overlying SML (Figs. 14A, 15A,B). Although the active cell velocity, w_{sb}, was important to maintaining the overall layer structure (Fig. 13), the turbulence-induced vertical velocities were most important to the individual cell trajectories (Fig. 14C). The 1-min rms vertical turbulent velocities were on the order of 10^1 mm s^{-1} in the core of the SML and 10^{-1}–10^0 mm s^{-1} in the layer, whereas w_{sb} peaked around $\sim 10^{-1}$ mm s^{-1} in the SML and was typically much smaller (Fig. 14C). Entrainment of cells from the layer into the SML was common (Fig. 14A). At the same time, retention of some cells within the layer was due largely to weak turbulent velocities at the base of the layer, rather than rapid swimming or sinking (Fig. 14A,C).

Cells positioned below the layer typically remained there, because w_{sb} and rms turbulent velocities were relatively weak (Figs. 14B,D, 15C). The rms vertical turbulent velocities were on the order of $\sim 10^{-1}$ mm s^{-1} and w_{sb}

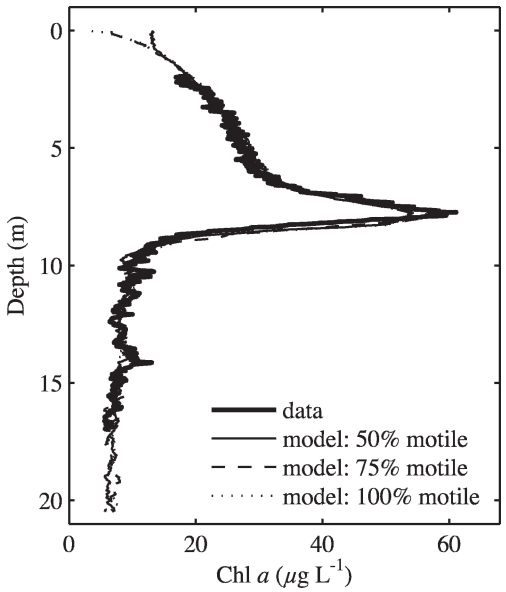

Fig. 13. Profiles of Chl *a* concentration from the Lagrangian particle-tracking model at steady state and the observed profile used to initialize it. The model was run with three different phytoplankton populations: (1) 50% motile and 50% passive; (2) 75% motile and 25% passive; and (3) 100% of the cells motile. The model profiles are 24-h mean profiles from the end of a 120-h model run period.

was typically a couple of orders of magnitude smaller (Fig. 14D). As a result, a minimal number of visits to the layer occurred from below.

The distribution of time spent within the layer (expressed as a percentage of total model run time) by individual cells is similar in shape for motile and passive cells, with low percentages of time much more frequent than high (Fig. 15). For comparison, we note that uniform sampling of the water column would lead cells to spend ~14% of their time in the layer based on the portion of the water column that it occupies. In general, motile cells spent more time within the layer as compared to passive cells (Fig. 15). For example, for cells initially above the layer, 49–66% of motile cells (depending on f_{motile}) spent more than a tenth of their time in the layer, compared to 31% for the passive cells (Fig. 15A). Still, many motile cells initially in the upper water column spent little time within the layer, indicating that the turbulence in the SML acted to suspend some cells despite the persistent downward cell velocity, w_{sb} (Fig. 15). Similar results are observed for cells initially within the layer (Fig. 15B), while cells within the lower water column (motile and passive) rarely accessed the layer (Fig. 15C).

In the upper water column and within the layer, an increase in the cell velocities, w_{sb} (corresponding to a reduction of f_{motile} in the model), produced an observable shift in the distribution of time spent within the layer towards higher values (Fig. 15A,B). However, the modest magnitude of the shift in response to variations in the vertical cell velocity further suggests that the turbulent motions were most important to the individual cell trajectories (Figs. 14, 15).

Layer breakdown—Finally, the breakdown phase of the thin layer was evaluated using the one-dimensional (vertical) Eulerian model without incorporating a convergence mechanism. The results indicate that the layer breaks down over a timescale of 10^1–10^2 h under the action of turbulent mixing alone (Fig. 8). The Chl *a* concentration peak of the layer is reduced by about 20 μg L^{-1} within 30 h and the Chl *a* gradients in the upper water column are completely erased after ~120 h.

Sullivan et al. (in press) observed the layer evolution to be on a diel cycle in Monterey Bay in 2005, in which mid-column layer formation initiated via downward migration of *Akashiwo sanguinea* to the thermocline in the late afternoon and ceased as these dinoflagellates migrated back to the sea surface in the early morning. Thus, pure turbulent diffusion was likely not the sole layer breakdown mechanism. The long (10^1–10^2 h) timescale of turbulence-forced layer breakdown from the model suggests that out-migration from the layer may indeed be required to maintain a diel periodicity to the mid-column layer formation–breakdown cycle.

Discussion

The present work highlights the value of simultaneous, microscale measurements of turbulence and planktonic distributions in the study of thin layers. The detailed measurements enabled inferences of the vertical dynamics of phytoplankton and an evaluation of the potential roles of various processes in thin-layer development, including swimming, buoyancy, growth, and, to a lesser extent, straining. Using the observations and inferences to force numerical models, we obtained a more complete description of the implications of various convergence–divergence balances on the dynamics and development of the thin layer and the vertical motions of individual cells. In future thin-layer studies, the coupling of turbulence-based inferences with direct measurements of layer species composition, growth conditions, and the timescales of formation and breakdown may allow for a more definitive assessment of the role of particular mechanisms in regulating layer dynamics.

The detailed measurements showed that the upper half of the thin layer was subjected to relatively strong mixing from the SML, which resulted in a relatively weak Chl *a* gradient. This strong mixing would have acted to entrain highly concentrated layer waters into the overlying SML, acting to diffuse the layer. The inferred vertical velocity needed to compensate for this diffusion is primarily on the order of 10^{-3}–10^{-2} mm s^{-1}. These inferred velocities are within the estimates of the sinking and swimming speed of *Akashiwo sanguinea* (Kamykowski et al. 1992; Park et al. 2002). Thus, either sinking or swimming could have provided the downward velocity. The lower half of the layer, on the other hand, experienced weak mixing that was associated with a very strong Chl *a* gradient. The upward vertical velocity needed to maintain this gradient in the presence of turbulent diffusion is on the order of 10^{-4}–10^{-3} mm s^{-1}. Cell sinking cannot produce such an upward velocity and the required mid-column convergence to

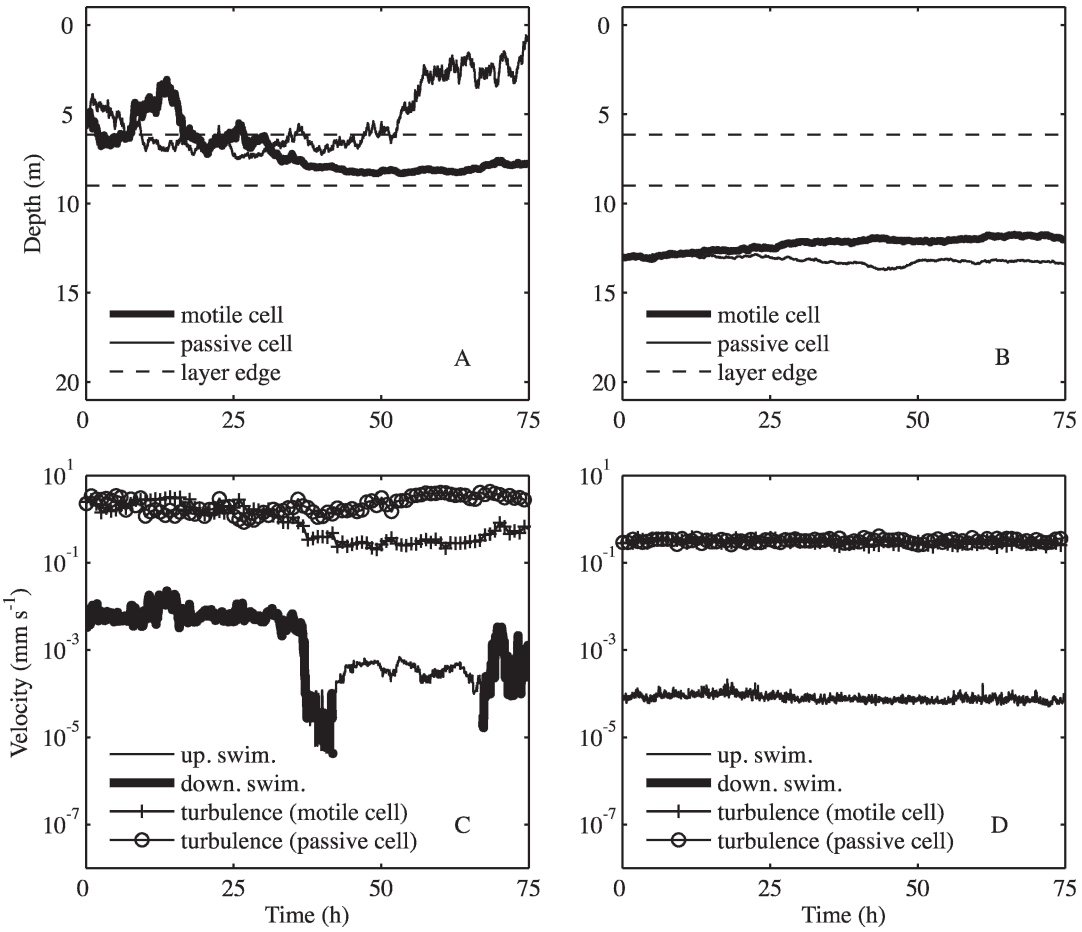

Fig. 14. (A) Two sample trajectories (of 10,000 trajectory realizations) for cells in the upper portion of the water column during a 75-h period of a Lagrangian particle-tracking model run. The trajectories were taken from the model scenario in which 75% of the cells were motile (migrating towards the layer center), while 25% were passively transported by turbulence. The type of cell (motile or passive) is indicated. The edges of the target layer are overlaid. (C) Vertical velocities associated with swimming (both upward and downward) and turbulence (1-min rms vertical turbulent velocities) for each of the cells in panel (A). (B, D) Same as panels (A, C) for two cells located in the lower portion of the water column.

maintain the thin layer, while upward swimming by *A. sanguinea* can explain both.

The asymmetry in the vertical structure may be a relatively common feature of thin layers in general. The observed asymmetry in the present study, apparent in a persistent layer of O(1 m) vertical dimension, was linked to vertically variable rates of diffusion about the pycnocline. Given that thin layers are typically observed in pycnoclines (Dekshenieks et al. 2001; Alldredge 2002; McManus et al. 2003) that often feature differential mixing, asymmetric layers may be quite common. Depending on the details of the vertical structure of turbulence and the biological distribution, differential mixing may act to relax or enhance the concentration gradients of a thin layer. The differential mixing may also imply asymmetries in the convergence mechanisms that act to form and maintain thin layers, as illustrated in the present study. A number of processes may provide such one-sided or asymmetric fluxes of biological material, including particle buoyancy, phototaxis, chemotaxis, and turbotaxis (Franks 2001; Alldredge et al. 2002). It is important to note that these biological mechanisms may produce thin-layer asymmetries in the absence of differential mixing and may also play a primary role in observed vertical asymmetries of plankton patches occurring over shorter time and spatial scales (O[10 min], O[10^{-1} m]; Mitchell et al. 2008).

Using a one-dimensional Eulerian advection–diffusion model, the timescales of layer development were evaluated for various candidate formation mechanisms. Inferences of Chl *a* production rates associated with phytoplankton growth implied a mid-column layer formation timescale of days, which is longer than observed by other researchers in the LOCO study (Sullivan et al. in press). Further, the inferred in-layer Chl *a* production rates were larger than expected for *A. sanguinea* and, thus, the model likely underestimated the time required for layer formation. Although in-layer growth was not likely a dominant mechanism for controlling layer dynamics over 10s of hours, growth may have still played an important role in controlling layer occurrence on longer timescales (e.g., days to weeks). Resource utilization gained by vertical migration and the formation of layers, for example, may stimulate

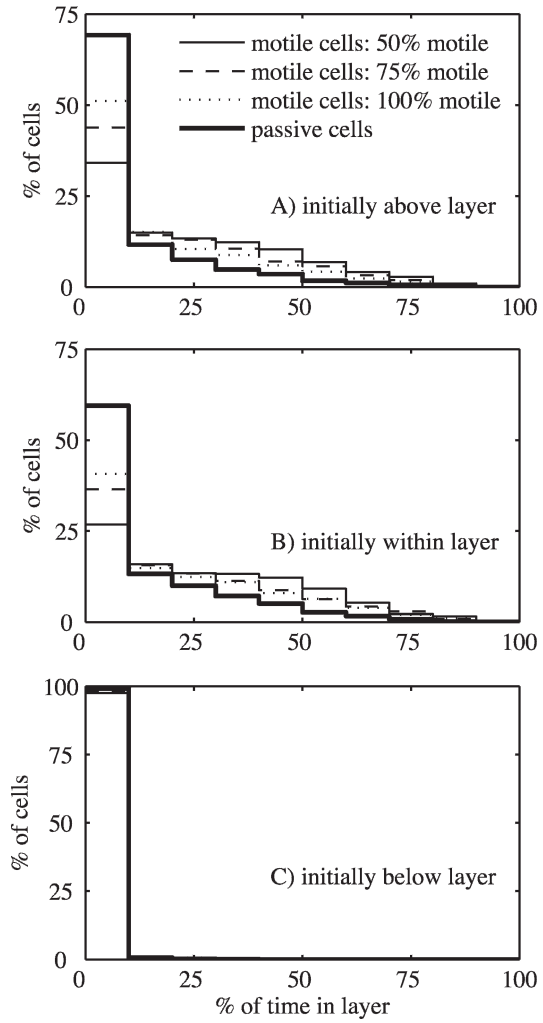

Fig. 15. Histograms of cumulative time spent by cells in the Chl *a* layer, expressed as a percentage of the total model run time. The Lagrangian particle-tracking model was initialized with an observed Chl *a* profile (seeded with 10,000 cells) and was maintained in a steady state for three different phytoplankton populations: (1) 50% motile and 50% passive; (2) 75% motile and 25% passive; and (3) 100% motile (Fig. 13). For each population scenario, the histograms are shown for the motile cells. For comparison, the histogram for the passive cells (same for all population scenarios) is also shown. The histograms are segmented as follows: (A) cells initially above the layer, (B) cells initially within the layer, and (C) cells initially below the layer.

growth and perpetuate the layer-forming phytoplankton population.

The Eulerian model results indicated that the layer formation process forced by vertical velocities inferred from the observations would also be on the order of days. Thus, elevated swim speeds are needed to explain more rapid layer formation. For example, a downward swim rate of 5%, 10%, and 20% of the potential swim speed of *A. sanguinea* (3×10^{-1} mm s^{-1}) above the layer centerline can produce the Chl *a* peak of the layer within hours, which is more consistent with the observed timescales of mid-column layer formation by Sullivan et al. (in press). The implication is that the cell motions may have taken on two distinct phases: rapid downward migration during formation, followed by relaxed vertical movement during layer maintenance. The Eulerian model also revealed that in the absence of a convergence mechanism, the layer would break down under the action of turbulent diffusion on a timescale of 10^1–10^2 h, though intermittent bursts of more intense mixing (e.g., in strong wind events or convection) could result in more rapid breakdown. Given that mid-column phytoplankton layers were observed to occur within a diel formation–breakdown cycle (Sullivan et al. in press), our results suggest that, in addition to turbulent diffusion, active migration out of the layer may have played a significant role in mid-column layer breakdown.

Finally, a Lagrangian particle-tracking model allowed for an investigation of the dynamics of individual cells within and around a steady thin layer. For a phytoplankton population consisting of ~50–100% motile cells migrating towards the mid-column, the layer structure could be maintained in a steady state while still satisfying individual cell swim speed constraints for *A. sanguinea*. The maintenance of the steady layer structure also supports the vertical velocity inferences used to force the Lagrangian model, which were derived from fits to the observed Chl *a* and K_z profiles. Analysis of the Lagrangian cell trajectories shows that the exchange of cells between the layer and vertically adjacent waters may have occurred primarily through the top of the layer, with a minimal number of cells exchanged at the base of the layer. This is due to the relatively high turbulent diffusivity and inferred swim speeds in the upper water column.

For an increase in the combined cell swimming-buoyancy velocities, there was a noticeable, but small, increase to the cumulative time spent within the mid-column layer. Although swimming was important to maintaining the vertical structure of the layer, the success of individual cells at maintaining vertical position within the mid-column depended largely on random, turbulent motions. Given that the phytoplankton layer was likely collocated with a nitracline, these results suggest that turbulent motions may play a dominant role in the growth success of individual cells, even with motility. Relatively weak turbulence within the mid-column, however, allowed some cells to persist within the layer before being entrained into the SML and potentially subjected to resource limitation (Ross and Sharples 2007, 2008). For organisms with greater swimming capabilities, such as copepods, plankter motions may be more independent of the turbulence field (Yamazaki and Squires 1996). For these organisms, the development and persistence of thin layers may be possible at higher rates of turbulent mixing.

Acknowledgments

We thank Brian McLaughlin, Matt Reidenbach, Jim Christmann, John Douglas, Peter Egli, Al Hanson, and Jan Rines for their contributions to this study, as well as a number of students from Stanford and University of California at Berkeley that participated in the fieldwork. Two anonymous reviewers contributed valuable comments that improved the quality of the manuscript. We gratefully acknowledge project support from the Office of Naval Research (N00014-04-1-04-1-0311), the Defense

University Research Instrumentation Program (N00014-05-1-0449), and the Friends of Long Marine Lab. JVS acknowledges student support from a National Defense Science and Engineering Graduate Fellowship and an Environmental Protection Agency Science to Achieve Results Fellowship.

References

Alldredge, A. L., and others. 2002. Occurrence and mechanisms of formation of a dramatic thin layer of marine snow in a shallow Pacific fjord. Mar. Ecol. Prog. Ser. **233:** 1–12.

Batchelder, H. P., C. A. Edwards, and T. M. Powell. 2002. Individual-based models of copepod populations in coastal upwelling regions: Implications of physiologically and environmentally influenced diel vertical migration on demographic success and nearshore retention. Prog. Oceanogr. **53:** 307–333.

Batchelor, G. K. 1959. Small-scale variation of convected quantities like temperature in turbulent fluid. J. Fluid Mech. **5:** 113–133.

Bearon, R. N., and D. Grünbaum. 2008. From individual behavior to population models: A case study using swimming algae. J. Theor. Biol. **251:** 679–697.

———, ———, and R. A. Cattolico. 2004. Relating cell-level swimming behaviors to vertical population distributions in Heterosigma akashiwo (Raphidophyceae), a harmful algae. Limnol. Oceanogr. **49:** 607–613.

———, and T. J. Pedley. 2000. Modelling run-and-tumble chemotaxis in a shear flow. Bull. Math. Biol. **62:** 775–791.

Birch, D. A., W. R. Young, and P. J. S. Franks. 2008. Thin layers of plankton: Formation by shear and death by diffusion. Deep-Sea Res. Part I. **55:** 277–295.

Carter, G. D., and J. Imberger. 1986. Vertically rising microstructure profiler. J. Atmos. Ocean. Technol. **3:** 462–471.

Carter, G. S., M. C. Gregg, and R.-C. Lien. 2005. Internal waves, solitary-like waves, and mixing on the Monterey Bay shelf. Cont. Shelf Res. **25:** 1499–1520.

Cheriton, O. M., M. A. McManus, D. V. Holliday, C. F. Greenlaw, P. L. Donaghay, and T. J. Cowles. 2007. Effects of mesoscale physical processes on thin zooplankton layers at four sites along the west coast of the U.S. Estuar. Coasts **30:** 1–16.

———, ———, M. T. Stacey, and J. V. Steinbuck. 2009. Physical and biological controls on the maintenance and dissipation of a thin phytoplankton layer. Mar. Ecol. Prog. Ser. **378:** 55–69.

Cloern, J. E., and R. Dufford. 2005. Phytoplankton community ecology: Principles applied in San Francisco Bay. Mar. Ecol. Prog. Ser. **285:** 11–28.

———, C. Grenz, and L. Vidergar-Lucas. 1995. An empirical model of the phytoplankton chlorophyll:carbon ratio—the conversion factor between productivity and growth rate. Limnol. Oceanogr. **40:** 1313–1321.

Cowles, T. J., R. A. Desiderio, and M.-E. Carr. 1998. Small-scale planktonic structure: Persistence and trophic consequences. Oceanography **11:** 4–9.

Dekshenieks, M. M., P. L. Donaghay, J. M. Sullivan, J. E. B. Rines, T. R. Osborn, and M. S. Twardowski. 2001. Temporal and spatial occurrence of thin phytoplankton layers in relation to physical processes. Mar. Ecol. Prog. Ser. **223:** 61–71.

Doucette, G. J., and P. J. Harrison. 1990. Some effects of iron and nitrogen stress on the red tide dinoflagellate *Gymnodinium sanguineum*. Mar. Ecol. Prog. Ser. **62:** 293–306.

Franks, P. J. S. 1995. Thin layers of phytoplankton: A model of formation by near-inertial wave shear. Deep-Sea Res. Part I. **42:** 75–91.

———. 2001. Turbulence avoidance: An alternative explanation of turbulence-enhanced ingestion rates in the field. Limnol. Oceanogr. **46:** 959–963.

Gibson, C. H., and W. H. Schwartz. 1963. The universal equilibrium spectra of turbulent velocity and scalar fields. J. Fluid Mech. **16:** 365–384.

Graham, W. M., and J. L. Largier. 1997. Upwelling shadows as nearshore retention sites: The example of northern Monterey Bay. Cont. Shelf Res. **17:** 509–532.

Itsweire, E. C., J. R. Koseff, D. A. Briggs, and J. H. Ferziger. 1993. Turbulence in stratified shear flows: Implications for interpreting shear-induced mixing in the ocean. J. Phys. Oceanogr. **23:** 1508–1521.

Ivey, G. N., and J. Imberger. 1991. On the nature of turbulence in a stratified fluid. Part I: The energetics of mixing. J. Phys. Oceanogr. **21:** 650–658.

Johnson, K. S., and J. A. Needoba. 2008. Mapping the spatial variability of plankton metabolism using nitrate and oxygen sensors on an autonomous underwater vehicle. Limnol. Oceanogr. **53:** 2237–2250.

Kamykowski, D., E. J. Milligan, and R. E. Reed. 1998. Relationships between geotaxis/phototaxis and diel vertical migration in autotrophic dinoflagellates. J. Plankton Res. **20:** 1781–1796.

———, R. E. Reed, and G. J. Kirkpatrick. 1992. Comparison of sinking velocity, swimming velocity, rotation and path characteristics among six marine dinoflagellate species. Mar. Biol. **113:** 319–328.

———, and H. Yamazaki. 1997. A study of metabolism-influenced orientation in the diel vertical migration of marine dinoflagellates. Limnol. Oceanogr. **42:** 1189–1202.

Kessler, J. O. 1986. Individual and collective fluid dynamics of swimming cells. J. Fluid Mech. **173:** 191–205.

Kiørboe, T., H.-P. Grossart, H. Ploug, K. Tang, and B. Auer. 2004. Particle-associated flagellates: Swimming patterns, colonization rates, and grazing on attached bacteria. Aquat. Microb. Ecol. **35:** 141–152.

Kundu, P. K., and I. M. Cohen. 2004. Fluid mechanics, 3rd ed. Cambridge Univ. Press.

Luketina, D. A., and J. Imberger. 2001. Determining turbulent kinetic energy dissipation from Batchelor curve fitting, J. Atmos. Ocean. Technol. **18:** 100–113.

McManus, M. A., and others. 2003. Characteristics, distribution and persistence of thin layers over a 48 hour period. Mar. Ecol. Prog. Ser. **261:** 1–19.

———, O. M. Cheriton, P. J. Drake, D. V. Holliday, C. E. Greenlaw, C. D. Storlazzi, and P. L. Donaghay. 2005. Effects of physical processes on structure and transport of thin zooplankton layers in the coastal ocean. Mar. Ecol. Prog. Ser. **301:** 199–215.

———, R. M. Kudela, M. W. Silver, G. F. Steward, P. L. Donaghay, and J. M. Sullivan. 2008. Cryptic blooms: Are thin layers the missing connection? Estuar. Coasts **31:** 396–401.

Mitchell, J. G., H. Yamazaki, L. Seuront, F. Wolk, and H. Li. 2008. Phytoplankton patch patterns: Seascape anatomy in a turbulent ocean. J. Mar. Syst. **69:** 247–253.

Osborn, T. R. 1980. Estimates of the local rate of vertical diffusion from dissipation measurements. J. Phys. Oceanogr. **10:** 83–89.

Park, M. G., S. K. Cooney, J. S. Kim, and D. W. Coats. 2002. Effects of parasitism on diel vertical migration, phototaxis/geotaxis, and swimming speed of the bloom-forming dinoflagellate *Akashiwo sanguinea*. Aquat. Microb. Ecol. **29:** 11–18.

Ross, O. N., and J. Sharples. 2004. Recipe for 1-D Lagrangian particle tracking models in space-varying diffusivity. Limnol. Oceanogr. Methods **2:** 289–302.

———, and ———. 2007. Phytoplankton motility and the competition for nutrients in the thermocline. Mar. Ecol. Prog. Ser. **347:** 21–38.

———, and ———. 2008. Swimming for survival: The role of phytoplankton motility in turbulent environments. J. Mar. Syst. **70:** 248–262.

Ruddick, B., A. Ayal, and K. Thompson. 2000. Maximum likelihood spectral fitting: The Batchelor spectrum. J. Atmos. Ocean. Technol. **17:** 1541–1555.

Ryan, J. P., M. A. McManus, J. D. Paduan, and F. P. Chavez. 2008. Phytoplankton thin layers caused by shear in frontal zones of a coastal upwelling system. Mar. Ecol. Prog. Ser. **354:** 21–34.

Sharples, J. 2008. Potential impacts of the spring-neap cycle on shelf sea primary production. J. Plankton Res. **30:** 183–197.

Stacey, M. T., M. A. McManus, and J. V. Steinbuck. 2007. Convergences and divergences and thin layer formation and maintenance. Limnol. Oceanogr. **52:** 1523–1532.

Steinbuck, J. V., M. T. Stacey, and S. G. Monismith. In press. An evaluation of χ_T estimation techniques: Implications for Batchelor fitting and ε. J. Atmos. Ocean. Technol.

Sullivan, J. M., P. L. Donaghay, and J. E. B. Rines. In press. Coastal thin layer dynamics: Consequences to biology and optics. Cont. Shelf Res.

Visser, A. W. 1997. Using random walk models to simulate the vertical distribution of particles in a turbulent water column. Mar. Ecol. Prog. Ser. **158:** 275–281.

Yamazaki, H., and K. D. Squires. 1996. Comparison of oceanic turbulence and copepod swimming. Mar. Ecol. Prog. Ser. **144:** 299–301.

Associate editor: Thomas Kiørboe

Received: 18 July 2008
Accepted: 16 February 2009
Amended: 03 April 2009